

Article

Improving Cycle Life of Silicon-Dominant Anodes Based on Microscale Silicon Particles under Partial Lithiation

Stefan Haufe , Johanna Ranninger, Rebecca Bernhard, Irmgard Buchberger and Eckhard Hanelt

Wacker Chemie AG, Consortium für Elektrochemische Industrie, Zielstattstr. 20, 81379 Munich, Germany

* Correspondence: stefan.haufe@wacker.com

Abstract: Using only parts of the maximum capacity of silicon microparticles in a lithium-ion battery (LIB) anode represents a promising material concept. The high capacity, better rate capability compared with graphite and accessibility on an industrial scale, as well as its attractive cost make microsilicon an ideal choice for the next generation anode material. However, currently the cycle life of LIBs using silicon particles in the anode is limited due to drastic volume change of Si during lithiation and delithiation. Continuous formation of a solid electrolyte interphase (SEI) and the associated lithium loss are the main failure mechanisms, while particle decoupling from the conductive network plays a role mainly during operation at low discharge voltages. The present study discusses approaches on the material- and cell-level to enhance cycle performance of partially lithiated silicon microparticle-based full cells by addressing the previously described failure mechanisms. Reducing the surface area of the silicon particles and coating their surface with carbon to improve the electronic contact, as well as prelithiation to compensate for lithium losses have proven to be the most promising approaches. The advantageous combination of these routes resulted in a significant increase in cycling stability exceeding 600 cycles with 80% capacity retention at an initial capacity of about 1000 mAh g⁻¹ at anode level, compared to only about 250 cycles for the non-optimized full cell.

Keywords: lithium-ion battery; silicon microparticles; partial lithiation; prelithiation; carbon coating; fines removal; LiNO₃ treatment



Citation: Haufe, S.; Ranninger, J.; Bernhard, R.; Buchberger, I.; Hanelt, E. Improving Cycle Life of Silicon-Dominant Anodes Based on Microscale Silicon Particles under Partial Lithiation. *Batteries* **2023**, *9*, 58. <https://doi.org/10.3390/batteries9010058>

Academic Editor: Dong Liu

Received: 6 December 2022

Revised: 9 January 2023

Accepted: 11 January 2023

Published: 13 January 2023



Copyright: © 2023 by the authors. Licensee MDPI, Basel, Switzerland. This article is an open access article distributed under the terms and conditions of the Creative Commons Attribution (CC BY) license (<https://creativecommons.org/licenses/by/4.0/>).

1. Introduction

Silicon is one of the most promising anode materials for high energy density LIB cells due to the high electrochemical capacity of Li₁₅Si₄ with 3579 mAh g⁻¹, which is about ten times the capacity of graphite [1,2]. However, so far, the application of silicon in LIB anodes has been limited because of the huge volume expansion of Si during lithiation, which can reach up to 300% and can be ascribed to the amorphization of Si and conversion into a Li_xSi_y alloy with high lithium content [3–5]. In general, the large volume change of Si particles during lithiation and delithiation leads to three previously described challenges [4] that need to be solved for a broad market introduction of silicon-dominant anodes. Firstly, mechanical stress leads to electrochemical milling of silicon particles, which can interrupt the electronic contact between silicon particles and/or the current collector. As a result, the decoupled particles can no longer contribute to the active capacity of the anode. It has been shown that pulverization is only relevant for Si particles larger than 100 nm. Nanoparticles smaller than 100 nm are not affected by this particular degradation mechanism [6–8]. Secondly, the mechanical strain on the binder weakens the entire anode structure, which also impairs the electronic contact between the silicon particles and the current collector but can destabilize and damage the anode structure. Both lead to a rapid decrease in capacity. Thirdly, the enormous volume expansion of silicon leads to cracks in the SEI layer, which results in newly exposed Si surface to the electrolyte, where new SEI is formed. During this process active lithium and electrolyte components are continuously consumed in each cycle, which also results in capacity fading [4,9,10].

In an attempt to limit rapid capacity fading due to high initial and continuous active lithium losses, different material concepts for optimized anode active materials have been investigated and described in the literature [11–18]. These concepts include silicon suboxide, nanostructured or porous silicon structures and silicon alloys. Additionally, Si/carbon composite systems have demonstrated significant improvements regarding decreased volume change and thus better cycle stability. However, production of such compounds usually requires lengthy synthetic pathways, often involving hazardous and expensive chemicals, which drive up the costs of the final product. Another approach to mitigate the large volume change is to use only part of the maximum available capacity of silicon microparticles, instead of the full 3579 mAh g^{-1} . With this strategy it is possible to limit the volume change and associated degradation mechanisms significantly [19–24].

This approach is worth considering because anodes with high capacities and good rate capability can be achieved. Furthermore, Si microparticles are accessible on an industrial scale, can be processed at existing cell production lines and represent an attractive alternative regarding costs. However, insufficient cycling stability and larger volume change during cycling limit the application of Si microparticles to fields where only moderate cycle life is required. In a recent study [25], continuous formation of SEI was identified as the dominant failure mechanism, while other degradation mechanisms, such as particle decoupling from the conductivity electrode network, come into play when low cut-off voltages are applied. Consequently, strategies of increasing cell performance [26] are based on optimizing the electronic connection between Si particles [4], reducing the material surface area, developing improved electrolyte systems [27–29] and/or prelithiation strategies [30–35]. Each of these strategies has been studied in detail but not yet optimized for the partially lithiated microsilicon and applied together to improve its electrochemical stability. In this study, some approaches to increase cycle life are highlighted and the effects of the individual measures as well as the synergistic combinations thereof are discussed. The techniques include removal of fines in the raw material, coating of the Si particles with carbon, addition of LiNO_3 to the cell and electrochemical prelithiation.

2. Materials and Methods

2.1. Material Preparation

2.1.1. Materials

All chemicals were obtained from commercial sources and were used as received unless otherwise noted. LiNO_3 (anhydrous), LiOH monohydrate and polyacrylic acid (PAA, 35 wt. % in water) were obtained from Sigma Aldrich (Darmstadt, Germany). KS6L and Super C65 from Imerys (Bodio, Switzerland) were utilized as conductive additives. Grade 1380 sodium carboxymethyl cellulose (NaCMC) from Daicel (Osaka, Japan) was used as dispersant. Lithium foil (0.5 mm) was purchased from Albemarle Corp. (Charlotte, NC, USA), copper foil (SE-Cu58, 20 μm) from Carl Schlenk AG (Bavaria, Germany). LiPF_6 as conductive salt was delivered by Advance Research Chemicals (Catoosa, OK, USA). The electrolyte solvents diethyl carbonate (DEC), ethylene carbonate (EC) and fluoroethylene carbonate (FEC) were obtained from Gotion (Fremont, CA, USA). All other materials used in the experiments are described in the subsequent sections.

2.1.2. Preparation of Silicon Microparticles (CLM00001)

Silicon lumps (5000 g) in photovoltaic purity (9 N) were loaded into a CGS-16 jet mill (NETZSCH Trockenmahltechnik GmbH, Germany). The grinder was operated with hot and compressed air ($95 \text{ m}^3 \text{ h}^{-1}$, $200 \text{ }^\circ\text{C}$ at 7 bar). The integrated classifier was set to 5800 rpm. In a second step, the fine fraction of the resulting silicon powder was removed in an air classifier CFS 8HD-S (NETZSCH Trockenmahltechnik GmbH, Hanau, Germany) at 7900 rpm. As shown in Figure 1 and corresponding Table 1, the silicon powders obtained had particle size distributions (PSD) weighted by volume with percentiles of $d_{10} = 0.8 \text{ }\mu\text{m}$, $d_{50} = 4.4 \text{ }\mu\text{m}$ and $d_{90} = 9.3 \text{ }\mu\text{m}$ for standard/non-classified and $d_{10} = 2.6 \text{ }\mu\text{m}$, $d_{50} = 5.7 \text{ }\mu\text{m}$ and $d_{90} = 9.9 \text{ }\mu\text{m}$ for air classified. The surface, measured by BET, was $2.8 \text{ m}^2 \text{ g}^{-1}$ after

milling and $1.5 \text{ m}^2 \text{ g}^{-1}$ after removing the fine fraction. The oxygen content after passivation treatment was 0.4 wt. %.

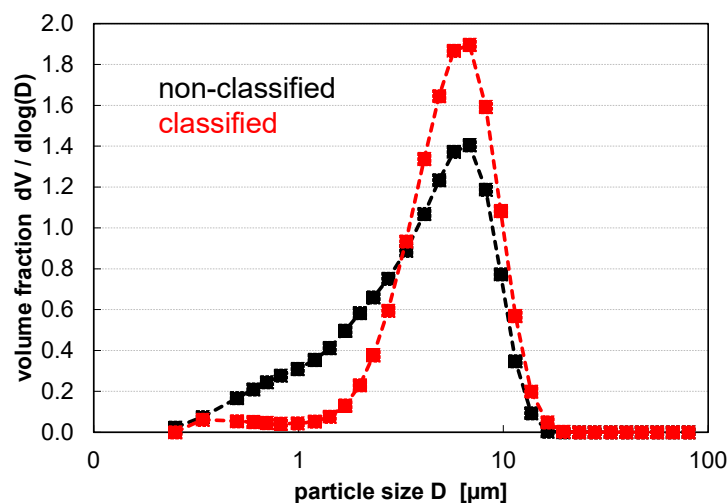


Figure 1. Particle size distributions of silicon microparticles (CLM00001) before and after air classification showing the removal of fines.

Table 1. Particle properties of CLM00001 before and after air classification showing a shift to larger particle sizes and lower material surfaces.

	d_{10} in μm	d_{50} in μm	d_{90} in μm	Span = $(d_{90} - d_{10})/d_{50}$	BET in $\text{m}^2 \text{ g}^{-1}$
Standard PSD	0.83	4.35	9.31	1.95	2.79
Air classified PSD	2.60	5.67	9.90	1.29	1.48

2.1.3. Preparation of Carbon Coated Silicon Microparticles (CLM00007)

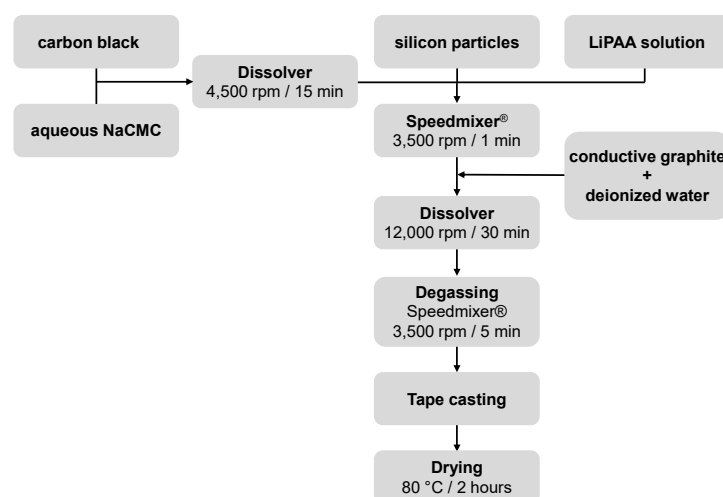
Silicon powder (20.00 g) and pitch (Rain Carbon, Germany, Petromasse ZL 250M, ATE21301) 1.05 g (5.0 wt. %), 1.54 g (7.0 wt. %) or 2.22 g (10.0 wt. %) were mixed mechanically by means of a ball mill roller bed (Siemens/Groschopp, Viersen, Germany) at 80 rpm for 3 h. The Si/pitch mixture was introduced into a quartz glass boat (QCS GmbH, Moerfelden-Walldorf, Germany) and carbonized in a three-zone tubular furnace (TF3 12/60/600, Carbolite GmbH, Neuhausen, Germany) using cascade control with an N-type sample thermocouple and Ar as inert gas. The temperature program started with a heating speed of $5 \text{ }^\circ\text{C min}^{-1}$ up to a temperature of $350 \text{ }^\circ\text{C}$. This temperature was held for 30 min to ensure that the pitch was completely melted. In the next step, heating was continued to $550 \text{ }^\circ\text{C}$ at a heating speed of $3 \text{ }^\circ\text{C min}^{-1}$, followed by a heating speed of $10 \text{ }^\circ\text{C min}^{-1}$ until the final temperature of $1000 \text{ }^\circ\text{C}$ was reached and held for 2 h. The product was left to cool down under argon overnight. After cooling, the carbon coated Si was sieved (mesh size $20 \text{ } \mu\text{m}$) to separate agglomerates from the final product. The carbon content for the different pitch admixtures, particle size distributions and densities for the corresponding anodes with carbon coated Si are shown in Table 2. Based on the BET surface area of the non-classified silicon and an assumed density of the amorphous carbon layer of 1.8 g cm^{-3} , the calculated average layer thickness at the highest C content was about 12 nm.

Table 2. Particle properties of CLM00007 based on non-classified CLM00001 showing increasing particle aggregation with rising carbon content.

Carbon in wt. %	d ₁₀ in μm	d ₅₀ in μm	d ₉₀ in μm	Span = (d ₉₀ - d ₁₀)/d ₅₀	Density in g cm ⁻³
0.0	0.83	4.35	9.31	1.95	0.95
2.3	1.79	6.46	14.02	1.89	0.84
4.0	2.82	7.63	15.97	1.72	0.81
5.7	3.03	8.51	17.86	1.74	0.75

2.1.4. Anode Preparation Using Silicon Microparticles

The silicon anodes contained 70.0 wt. % silicon microparticles, 20.0 wt. % KS6L conductive graphite, 2.0 wt. % Super C65 carbon black, as well as 7.8 wt. % LiPAA and 0.2 wt. % NaCMC as binder or dispersant. According to the process diagram in Figure 2, a conductive additive solution was prepared in a first process step. For this purpose, 0.29 g of Super C65 carbon black was suspended in 3.30 g of aqueous NaCMC (0.87 wt. %) using a dissolver type DISPERMAT[®] LC30 (VMA-Getzmann GmbH, Reichshof, Germany). For the slurry preparation, 10.05 g of pure or carbon coated Si particles and 3.59 g of the conductive additive dispersion were mixed with 11.48 g of LiPAA solution in water (10 wt. % solids content, LiOH was used to neutralize the aqueous PAA solution to pH 7.0) in a Speedmixer[®] type DAC 150 SP (Hausschild GmbH & Co. KG, Hamm, Germany). Optimal rheology for the coating process results from thickening of the PAA solution during neutralization of the binder. After adding 2.87 g of conductive graphite (KS6L, Imerys, Bodio, Switzerland) and 4.43 g of deionized water, stirring was continued in the dissolver for 30 min at 12,000 rpm. The solids content of the final anode slurry was 41.1 wt. %. After devolatilization at 3500 rpm for 5 min in a Speedmixer[®], the suspension was evenly spread on a copper foil (20 μm) with a gap bar. The electrode was then dried at 80 °C for 2 h. The areal weight of the coating was 3.0 mg cm⁻² corresponding to a calculated capacity of 7.5 mAh cm⁻². Depending on the voltage window, about 30% of the capacity was used. The density of the electrode material containing the pure Si particles without subsequent calendaring was about 1.0 g cm⁻³ (see Table 2).

**Figure 2.** Process steps for preparation of the microsilicon-containing anodes.

2.1.5. Post-Treatment with LiNO₃

Impregnation of anode, cathode or separator was performed at ambient conditions by dropwise (30 μL) addition of an ethanolic LiNO₃ solution (0.22 g of LiNO₃ in 10 mL of water-free ethanol) evenly on the electrode surface. The solvent was vaporized at room temperature and the coating was then dried at 80 °C to constant weight. The maximum loading of nitrate was 1.5 mg cm⁻².

2.2. Material Testing

2.2.1. Full Cell Measurement

In order to ensure comparability with previous work, the same measurement conditions for the full cell testing were chosen [22,25]. The tests were performed in CR2032 button cells (Hohsen Corp., Tokyo, Japan) with an electrode diameter of 15 mm. The silicon coating on Cu foil was used as the negative electrode, and a coating of $\text{LiN}_{0.6}\text{Mn}_{0.2}\text{Co}_{0.2}\text{O}_2$ (NCM622) on Al foil with an active material content of 94.0 wt. % and an areal weight of 15.0 mg cm^{-2} (SEI Corp., Tsu, Japan) and 2.3 mAh cm^{-2} as reversible capacity was used as the positive electrode. The silicon capacity utilization in this arrangement corresponded to ~30% (N/P ratio of 3.3). The electrolyte was composed of a 1.0 M solution of LiPF_6 in a 4:1 mixture by volume of DEC and FEC. A glass fiber filter paper (Whatman, Maidstone, UK, GD type A/E) soaked with 60 μL of electrolyte (diameter 16 mm) was used as separator for material screening. Thanks to its flexibility, it can compensate for surface roughness in the case of slightly uneven electrodes. In addition, pouch cells were prepared with a $5.0 \times 5.0 \text{ cm}^2$ anode, a $5.5 \times 5.5 \text{ cm}^2$ cathode and a $6.0 \times 6.0 \text{ cm}^2$, 25 μm thick polypropylene-based separator (Celgard[®] 2500). The amount of electrolyte for the pouch cell format was 350 μL . At this point, the electrodes had a quality that allowed the use of a commercial separator.

Cells were built in a glove box (<5 ppm H_2O , O_2 , MBraun GmbH, München, Germany). Electrode and separator drying was performed under vacuum for at least 10 h at 120 °C and 180 °C, respectively, resulting in a water content in all components of less than 20 ppm.

All cycling tests were carried out at 22 °C using a CTS battery tester (BaSyTec GmbH, Asselfingen, Germany). Cells were charged using a *cc/cv* (constant current/constant voltage) method with C/10 (12 mA g^{-1}) in the formation cycle and C/2 (60 mA g^{-1}) in all subsequent cycles to a voltage cut-off of 4.2 V. At the voltage limit, charging continued until the current was below C/100 (1.2 mA g^{-1}) or C/50 (2.4 mA g^{-1}). The cells were discharged with C/10 (12 mA g^{-1}) in the formation cycle and with C/2 (60 mA g^{-1}) in the subsequent cycles to a voltage cut-off of 3.0 V or alternatively 2.5 V. The chosen current was based on the coating weight of the positive electrode. When a capacity retention of 70% was attained, the testing was automatically terminated.

2.2.2. Prelithiation of CLM00001- and CLM00007-Containing Anodes

Electrochemical prelithiation was carried out in the same cell formats as mentioned above, using the silicon anode as working electrode and a lithium foil (in the CR2032 cell) or a capacity-oversized NCM622 cathode (in the pouch cell) as counter electrode. All other cell components and the conditions used for preparation and testing were identical to above.

For prelithiation, the Si anode was lithiated at C/25 to 1050 mAh g^{-1} . Here, the value of the prelithiation level refers to the coating weight of the anode. After that, the anode was dealloyed at the same C-rate to 1.5 V. Finally, the anode was lithiated again at C/25 to the desired prelithiation level of up to 840 mAh g^{-1} . The portion of active material is about 70% of the coating weight of the anode. Thus, the final prelithiation level of the total anode corresponds to a level of up to 1200 mAh g^{-1} related to the anode active material.

3. Results and Discussion

By removing the fine fraction of CLM00001, it is possible to reduce the material surface area and thus, possibly, the loss of lithium due to new SEI formation during cycling. A narrower particle size distribution should also result in a more homogeneous particle lithiation under partial capacity use.

For powdered materials with a small particle size, such as CLM00001, the fines can be removed by air classification. As shown in Table 1, this narrows the particle size distribution, observable from the value for the span given by $(d_{90}-d_{10})/d_{50}$. The median d_{50} of the PSD, which is 4.5 μm for the standard CLM00001, is shifted to larger particles at 5.7 μm . The BET surface area is reduced by about 50% from 2.76 to 1.48 $\text{m}^2 \text{ g}^{-1}$. From an economic point of view, it should be noted that less than half of the air classified material is

produced in the same amount of time and the fine fraction of the ground material (up to 30%) must be discarded.

Figure 3 compares the discharge capacity of full cells with Si anodes based on standard and size modified CLM00001. In this and the following figures, the best curve out of a series of three cells is shown to illustrate the maximum effect of the respective modification. However, the other cells reflect the same trend. The cycle stability shown in the graph is enhanced by removing the fines and improves by about 50 cycles from 252 to 303 cycles at 80% capacity retention. It should be noted that it is not possible to differentiate whether less SEI re-formation is due to the reduced material surface or to a more homogeneous lithiation since the narrower PSD could influence both.

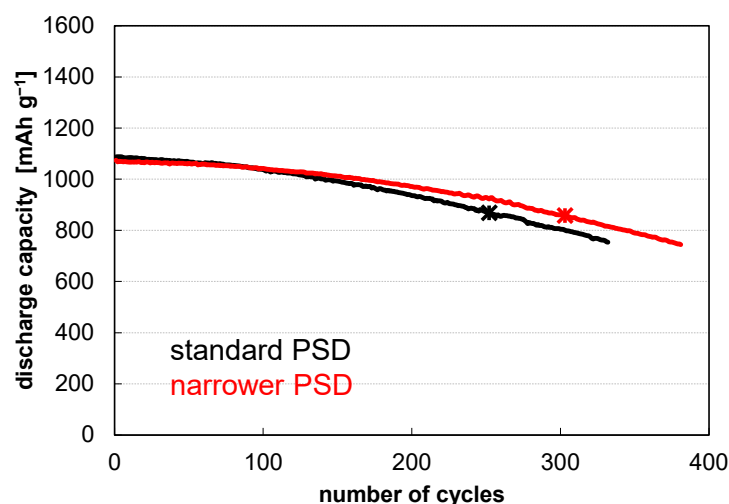


Figure 3. Cycling behavior of full cells (discharge capacity of anode active material) based on air classified (narrower) CLM00001 compared to unmodified (standard) CLM00001 in the 4.2–3.0 V range. The asterisks mark 80% capacity retention. The removal of fine particles moderately increases the cycle life in the 4.2–3.0 V range by about 50 cycles from 252 to 303 cycles.

Another path to enhance the electrochemical properties of CLM00001 is to coat the particle surface with carbon [36–39]. This should lead to a better electronic particle connection, especially with progressive delithiation of the anode material occurring at low discharge voltages of the full cell below 3.0 V. Under these conditions, the inner resistance of CLM00001-based cells increases sharply [25]. However, it can be assumed that a full surface coating will not withstand the volume expansion of about 100% at 1200 mAh g_{Si}⁻¹. At least a partial C-coating should be sufficient to improve the particle conductivity.

Table 2 shows the particle size distributions of carbon coated, non-classified CLM00001 (referred to as CLM00007) for different carbon contents. The percentiles of the particle size distribution increase with increasing carbon content. The PSD is narrowed indicating an increasing aggregation especially of small silicon particles by composite formation with carbon. The aggregation is also reflected in the density of the non-calendered electrode coating, which decreases with increasing carbon content from 0.95 g cm⁻² to 0.75 g cm⁻² at minimum (0.0% C) and maximum content (5.7% C), respectively.

Figure 4 shows an SEM cross section (magnification 30 k) of carbon coated CLM00007 (2.3 wt. % carbon) embedded in epoxy resin. The splinter-like nature of the base material CLM00001 is obvious. It can be observed that the coating leads to agglomerates and shows areas where the coating is more than 300 nm thick and other areas where no coating is visible with this technique. To test whether the carbon coating covers the Si particle fully or if it is incomplete, 1–2 g of CLM00001 and CLM00007 were soaked in 10 mL of ethanol and 10 mL of 4 N NaOH at 40 °C for 15 min. Bare Si is dissolved in NaOH under H₂ evolution and only 14 wt. % of the product can be recovered. However, for CLM00007 with 2.3 wt. % carbon content 97 wt. % can be recovered, which indicates an almost complete coverage of Si with a (protecting) C-layer. It should be noted here that a higher carbon content in the

anode active material does not have a significant effect on the mass recovery after treatment in alkaline solution (98% mass recovery at 5.7 wt. % carbon coating), but has a strong effect on particle aggregation, as indicated by increased values for PSD (see Table 2).

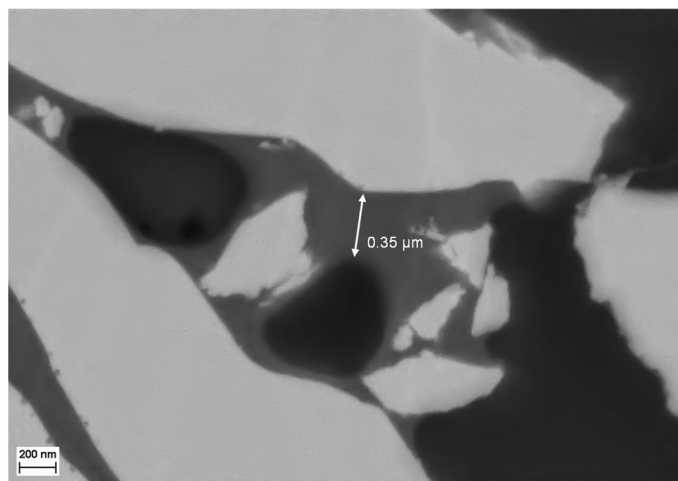


Figure 4. SEM cross section (magnification 30 k) of carbon coated CLM00007 (2.3 wt. % carbon) embedded in epoxy resin (Si: light gray region, C-coating: dark gray region, epoxy resin: black region). In the image, areas with very thick C-layers and Si particles sharing a C-layer are visible, which illustrates the formation of aggregates. This effect is also observed as an increase in the percentile values of the PSD (see Table 2). Thin C-layers (<20 nm) on the silicon surface are not visible in the present magnification.

In Figure 5, the cycle stability of full cells with Si anodes based on CLM00007 is depicted as a function of the carbon content for the voltage ranges 4.2–3.0 V and 4.2–2.5 V. Cycle life improves with carbon coating, particularly in the 4.2–2.5 V window, where the conductivity of the silicon particles is reduced by substantial delithiation at lower voltages. An improvement of up to 13% (from 249 to 281 cycles on average) is observed in the narrower voltage window and 42% (from 156 to 222 cycles) in the wider one. The improvement is particularly significant in the 4.2–2.5 V window because the conductivity of silicon decreases sharply with lower degree of lithiation (low discharge cut-off voltages) and the carbon coating minimizes the decoupling of the active material and the associated capacity loss.

The positive effect is already evident at the lowest selected carbon content of about 2 wt. %. This content is considered optimal, since a further increase in added pitch has no positive influence on cycle stability but leads to a stronger particle aggregation and reduced Si content in the anode. Additionally, more carbon coated Si is lost in the sieving process after the carbonization because the number of aggregates that are larger than 20 μm also increases. It is also worth noting that the cycle curves, on which Figure 5 is based, show that the carbon coating does not affect the starting capacity in a trend related to the C content (0.0–5.7% C: 1087–1065 mAh g^{-1} of anode active material for the 4.2–3.0 V range and 1192–1169 mAh g^{-1} for 4.2–2.5 V). Thus, the carbon coating does not provide a significant additional contribution to the irreversible initial capacity of the cell.

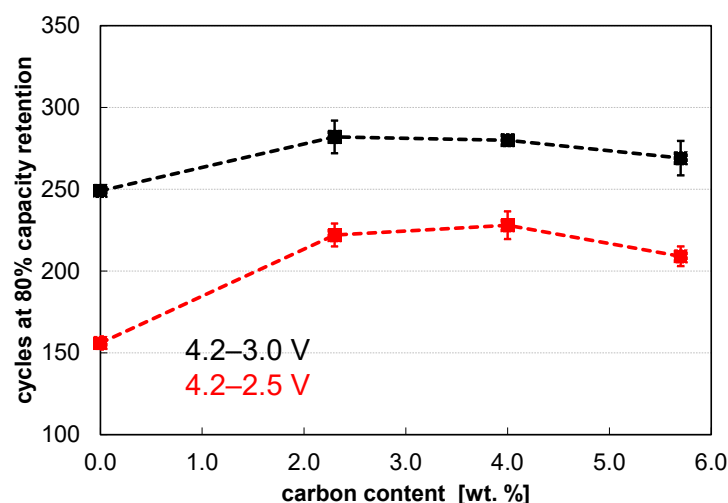


Figure 5. Cycle life (at 80% capacity retention) of full cells with silicon anodes based on carbon coated CLM00001 (standard PSD) as a function of carbon content. Cycle numbers represent mean values in a series of three cells, error bars indicate the standard deviation. The carbon coating improves the cycle life particularly in the 4.2–2.5 V window where the conductivity of the silicon particles is reduced by substantial delithiation at lower voltages.

An electrolyte-based approach to improve cycling stability is the addition of LiNO_3 to the cell. As discussed by Graf et al. [40], LiNO_3 is converted to LiNO_2 under reductive conditions (1.56 V vs. Li/Li^+), which is further reduced (1.39 V vs. Li/Li^+) to insoluble LiN_3 . XPS measurements show that LiN_3 is present in the SEI layer. In addition, LiNO_2 is oxidized at the cathode to gaseous NO_2 (3.5 V vs. Li/Li^+), which can be consumed upon reduction and further passivates the surface of the Si particles. In addition to LiNO_3 , other alkali nitrates or nitrites such as NaNO_3 , KNO_3 or LiNO_2 also have a positive influence on cycle life.

LiNO_3 is only very poorly soluble in common carbonate-based electrolytes with a content of <0.3 wt. %. Thus, only small quantities of LiNO_3 can be introduced with an optimized amount of electrolyte (1.5–3.0 mL Ah^{-1}). However, addition via the cell components represents a promising route to achieve higher content [27]. Since experiments to introduce LiNO_3 via the anode slurry had no positive effect, impregnation of the anode, cathode or separator with an ethanolic LiNO_3 solution (see experimental Section 2.1.5) was pursued.

Figure 6 shows the number of cycles at 80% capacity retention of full cells with CLM00001 anodes (standard PSD) and DEC/EC-based electrolyte as a function of the LiNO_3 loading, which was applied on the anode, cathode or separator (with error bars for the standard deviation in a series of three cells). The above electrolyte was chosen because the nitrate effect is quite distinct for this mixture. It was observed that the stability improves from about 100 cycles to 300 cycles with increasing nitrate content. For the impregnated anode or the separator side facing the anode, the maximum improvement is already evident at a loading of 0.25–0.35 mg cm^{-2} . In the case of the impregnated anode, the gain in cycles decreases again with higher loading. It cannot be excluded that the nitrate is not only introduced superficially via the ethanolic solution, but also penetrates the hydrophilic pore structure of the anode, progressively filling the pores and disturbing the electrolyte contact. Higher doping levels are required for the impregnated cathode, possibly because the point of application is not the effective point, i.e., the surface of the anode active material. A loading of 0.35 g cm^{-2} LiNO_3 (17 mg per 100 mg CLM00001) applied on the anode was chosen as the preferred level for subsequent investigations.

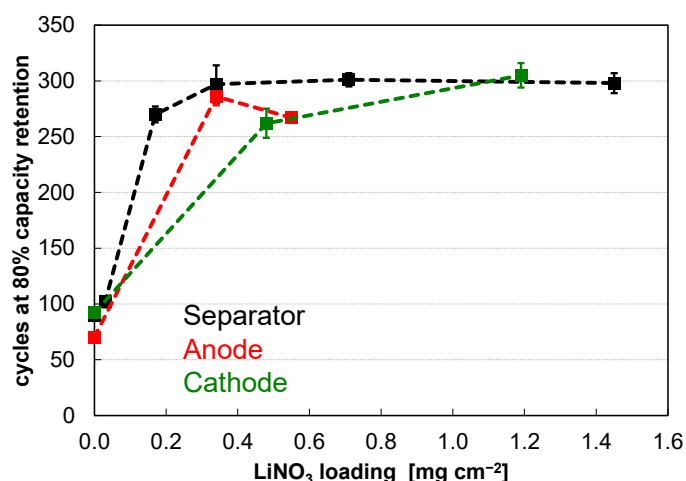


Figure 6. Cycle life (at 80% capacity retention) of full cells with CLM00001 anodes (standard PSD) and DEC/EC-based electrolyte as a function of the LiNO_3 loading applied on the anode, cathode or separator (4.2–3.0 V range). The increasing nitrate content improves stability from about 100 cycles to 300 cycles. Cycle numbers represent mean values in a series of three cells, error bars indicate the standard deviation.

Figure 7 presents the cycling behavior of CLM00001-based full cells with optimal LiNO_3 content for the DEC/EC- and DEC/FEC-electrolyte. The nitrate effect is also evident in the FEC-containing electrolyte. Although the cycle increase is not as pronounced as with the FEC-free electrolyte, an even higher cycle stability is achieved for this combination, with 316 cycles at 80% capacity retention. Consequently, the addition of LiNO_3 seems to improve cycle stability regardless of the electrolyte system chosen. However, a drawback of this electrolyte-related approach could be the continuous generation of NO gas on the cathode side, which could be potentially problematic in bigger cell formats, especially in pouch cells.

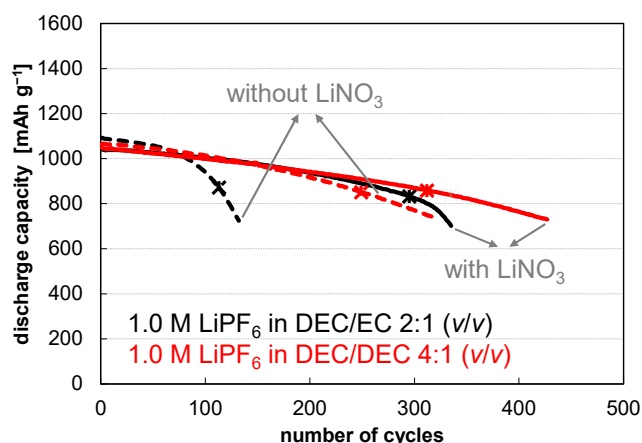


Figure 7. Cycling behavior of full cells (discharge capacity of anode active material) based on CLM00001 anodes (standard PSD) with optimal LiNO_3 loading of 0.35 g cm^{-2} and two different electrolytes (solid lines in black and red) compared to similar cells without LiNO_3 in the 4.2–3.0 V range (dotted lines in black and red). The asterisks mark 80% capacity retention. The nitrate effect is also evident when EC in the electrolyte is replaced by FEC.

Another approach to improve electronic particle attachment and to compensate for lithium losses is prelithiation of Si-containing anode materials. The concept of partial lithiation is ideal for this purpose, because large amounts of silicon are unused and thus sufficient storage capacity is available [30]. With an optimal capacity utilization of CLM00001 of about 30% for reversible lithium storage, the remaining part can be prelithiated without

Li plating. The electronic particle connection is improved because at low discharge voltages some lithium remains in the anode. Thus, the particles do not lose their electric conductivity in the uncharged state of the battery.

In Figure 8, the discharge capacity of full cells with prelithiated Si anodes based on standard CLM00001 is shown for different prelithiation levels in the 4.2–3.0 V range. The start capacity increases from 1028 mAh g⁻¹ without prelithiation to 1110 mAh g⁻¹ with prelithiation of 600–1200 mAh g⁻¹ related to the silicon weight. The increase of the start capacity indicates that less lithium from the cathode is lost by irreversible effects in the first cycle. Thus, the usage of the cathode capacity is improved under the selected cycling conditions. The cycle stability also increases steadily to 250 cycles at 90% capacity retention with increasing prelithiation up to 600 mAh g⁻¹, before dropping again at even higher prelithiation. At high prelithiation levels (>600 mAh g⁻¹) and thus high material utilization, pulverization of the silicon particles occurs [22]. Under the selected conditions, prelithiation with 600 mAh g⁻¹ seems to provide maximum stability gain.

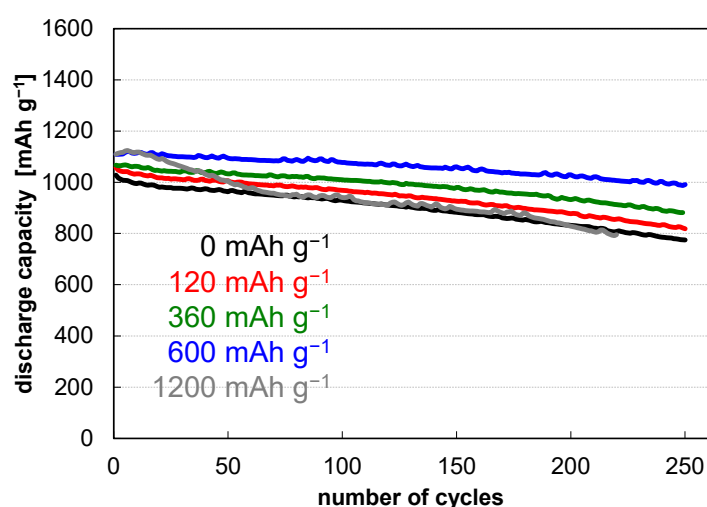


Figure 8. Cycling behavior of full cells (discharge capacity of anode active material) with prelithiated anodes based on standard CLM00001 with different prelithiation levels, voltage range 4.2–3.0 V. Appropriate prelithiation has been found to compensate for continuous lithium loss and strongly increases cycle life.

Figure 9 shows the long-term cycling of full cells based on CLM00001 with an optimal prelithiation content of 600 mAh g⁻¹ in different voltage windows. It is observed that the discharge capacity of full cells, whether prelithiated or not, is higher in the extended voltage window than that in the narrow one. This behavior can be explained by the sloping Si voltage profile [24], which causes lithium in the discharged battery to be trapped to some degree in the anode, depending on the voltage range. At low cut-off voltages (<3.0 V), more lithium is released, resulting in an increase in discharge capacity.

It can also be seen that the cycle life is greatly increased by prelithiation in both voltage windows with +168 and +291 cycles in the narrower and extended voltage window, respectively. The observed difference in stability of the non-carbon coated prelithiated CLM00001 and the non-prelithiated carbon coated CLM00007 (see Figure 5) in the extended voltage window can be explained by the fact that despite an improved electronic particle connection in both cases, only in the case of the prelithiated anode there is sufficient Li buffer over the entire cycle life to compensate for the losses due to the re-formation of SEI. The cycle numbers for prelithiated anodes in the narrow and extended voltage window are very similar. It can be argued that the failure mechanism of active lithium loss through SEI re-formation with prelithiated anodes is not the dominating degradation mechanism anymore because sufficient lithium reservoir is ensured [25]. Due to the high lithium content in Si, also the resistance of the anode at cut-off voltages below 3.0 V (wider

voltage window) is reduced in comparison to the non-prelithiated electrode, approaching full delithiation. A significantly higher increase in cycle numbers in the wider voltage window is observed compared to the narrow voltage window. It should be noted here that silicon has semiconducting properties and only the silicide Li_xSi with $x > 0.2$ show higher electronic conductivity [41].

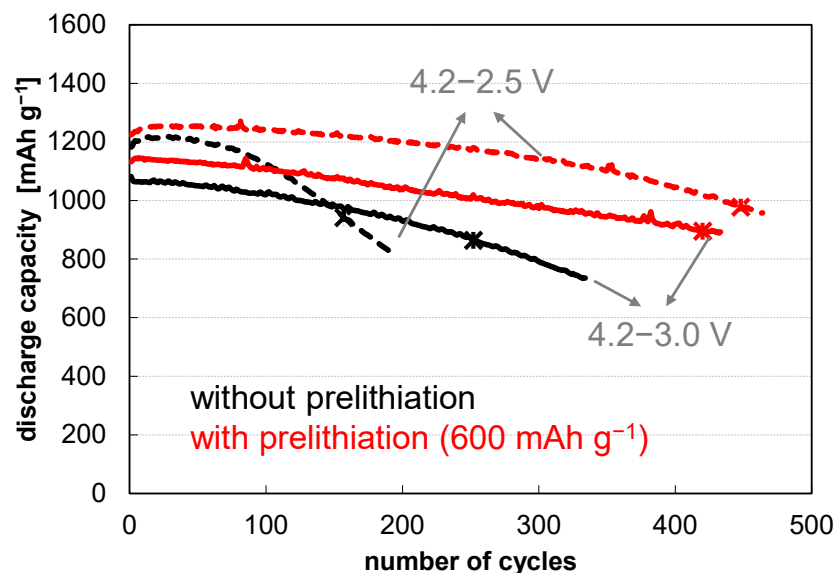


Figure 9. Cycling behavior of full cells (discharge capacity of anode active material) with prelithiated anodes based on standard CLM00001 with the optimal prelithiation level of 600 mAh g^{-1} in two different voltage windows. The asterisks mark 80% capacity retention. The cycle life for the 4.2–2.5 V range (dotted line) is slightly better than for the 4.2–3.0 V range (solid line). More than 440 cycles are possible in this configuration without carbon coating or classification.

Of all the approaches discussed, the prelithiation has the strongest positive effect on cycle life, demonstrating the great potential of this technique to enhance the cycling stability of Si-based anodes under partial lithiation. However, industrial implementation of prelithiation in large-volume cell production has not yet been achieved due to the reactivity of lithium, prelithiated anode materials or prelithiation reagents with water and oxygen and due to the resulting demanding processing equipment and safety precautions. Currently, different prelithiation techniques are under investigation and are evaluated according to their different fields of application and economic feasibility [31–33].

By combining the approaches listed above and considering synergistic effects, it should be possible to overcome the discussed limitations and significantly increase cycle stability. The interactions of different combinations were investigated to achieve maximum cycle stability. Table 3 shows the cycle life at 80% capacity retention in the 4.2–3.0 V window for the corresponding full cells. As previously mentioned, the removal of the fines content, carbon coating or LiNO_3 -treatment leads to a significant increase in stability of up to 64 cycles. Prelithiation is the most powerful approach with a gain of 168 cycles. The quantification refers to the cell with the best performance, as it shows the maximum potential of the respective combination. The mean value of the series of three cells also reflects the same trend.

Table 3. Cycle stabilities for combinations of the different optimization approaches (all electrolytes with DEC/FEC, 4.2–3.0 V window). The combination of prelithiation with carbon coated, size reduced CLM00001 allows more than 600 cycles. The cycle numbers at 80% capacity retention are given as mean values with standard deviation for a series of three cells and as maximum values.

Fines Removal	Carbon Coating	LiNO ₃ Treatment	Pre-Lithiation	Cycles @80% Retention
–	–	–	–	249 ± 04 252
+	–	–	–	292 ± 11 303
–	+	–	–	281 ± 11 289
–	–	+	–	311 ± 05 316
–	–	–	+	405 ± 15 420
+	–	–	+	467 ± 18 490
–	+	–	+	513 ± 19 531
–	–	+	+	411 ± 42 439
+	+	–	+	566 ± 32 603
+	+	+	+	578 ± 29 607

Since prelithiation appears to be essential for high cycle stability, this approach was combined with the others. As can be seen in Table 3, combinations show synergistic effects and enable stabilities of up to 531 cycles for prelithiation with a further modification. While the combination of prelithiation with fines removal or carbon coating results in a high stability of around 500 cycles, the additional LiNO₃ treatment causes only a moderate improvement to 439 cycles.

To further increase cycle life, prelithiation was combined with fines removal and carbon coating as the most efficient material approaches. According to the penultimate row of Table 3, more than 600 cycles were achieved for this combination. In contrast, the additional incorporation of LiNO₃ did not further improve stability (see last row).

To demonstrate the technical potential of the combinatorial approach, its transferability to 25 cm²-pouch cells was investigated. Figure 10 shows a comparison of the cycle stability of full cells based on prelithiated anodes with carbon coated and size reduced CLM00001, as the most effective combination, in coin cell and pouch cell formats in the voltage window 4.2–3.0 V. Transfer to the cell area 14 times larger in size was successful. The cells show similar starting capacities, and the pouch cell even shows a more stable cycling behavior (737 vs. 603 cycles). The reason for the higher cycle stability of the pouch cell can be explained by the use of the significantly thinner Celgard[®] separator (25 μm) compared to the thick Whatman[®] GF/A separator (260 μm) used in the coin cells. The voltage drop across the separator is thus reduced. Hence, the charge or discharge process can be more complete within the specified voltage window, especially at higher numbers of cycles where an increased resistance contribution of the grown SEI layer can be observed.

To enable high energy densities, material combinations with both high capacity and average discharge cell voltage are required. The pouch cell from Figure 10 has an average discharge voltage of 3.45 V at the start and 3.37 V at the end of life after 737 cycles. Compared to the rather stable mean discharge cell voltage of graphite-based cells of about 3.7 V over lifetime, this means that about 9% of the capacity gain is lost in energy density due to the voltage characteristics of the prelithiated CLM00007 anode compared to graphite.

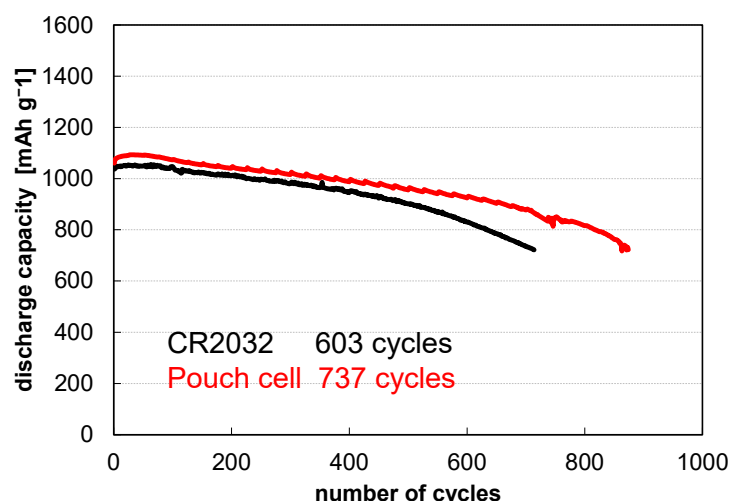


Figure 10. Cycling behavior of full cells (discharge capacity of anode active material) based on prelithiated anodes with carbon coated, classified CLM00001 in different cell formats. This combination allows more than 600 cycles at 80% capacity retention in the 4.2–3.0 V window.

4. Conclusions

The partial lithiation of silicon microparticles is a favorable approach to reach good rate capability and high capacity of lithium-ion batteries, while maintaining an attractive cost position.

However, low cycle stability (about 250 cycles) and significant volume change during lithiation currently limit its applications and market introduction. The continuous formation of SEI represents the main failure mechanism, while electronic particle decoupling comes into play when discharging to low discharge voltages.

In this study different methods to increase the cycle life of Si anodes using micro-sized particles under partial lithiation are discussed. These approaches are based on the reduction in silicon particle surface area, improving the electronic connection of Si particles within the electrode structure, the application of electrolyte additives and prelithiation. Specifically, the removal of the fines fraction from powdered silicon, carbon coating, addition of LiNO_3 as cell additive and electrochemical prelithiation were described as performance enhancing strategies.

Among the approaches discussed, prelithiation shows the strongest positive effect on cycle life (420 cycles). The lithium reservoir in the anode can compensate for the lithium losses until it is consumed, and thus provides stable cycling behavior. The combination of the methods of improvement described above results in synergistic effects that can further increase cycle life. More than 600 cycles were reached in the following best combination: fines removal, carbon-coating and prelithiation. In addition, the successful transfer to single-layer pouch cells was demonstrated.

With regard to technical feasibility, it should be noted that each additional process step increases the complexity of the production of LIB materials and cells and has a negative impact on the cost situation. While air classification and carbon coating are already used in manufacturing, post-treatment with LiNO_3 and prelithiation are not industrially established processes yet.

Nevertheless, it could be demonstrated that especially prelithiation has a great potential to significantly improve cycle stability, which should enable a broader market introduction. In combination with prelithiation, the partial lithiation of microscale silicon particles is an ideal approach to increase the volumetric energy density of LIB cells. In order to reach the goal of market introduction, more suitable electrolytes with significantly reduced SEI formation should be developed and the technical feasibility of prelithiation should be evaluated in more detail.

Author Contributions: Conceptualization, S.H. and J.R.; methodology, J.R., R.B., I.B. and E.H.; investigation, J.R., R.B., I.B. and E.H.; writing—original draft preparation, S.H. and J.R.; writing—review and editing, S.H., J.R. and E.H.; visualization, S.H.; supervision, S.H. All authors have read and agreed to the published version of the manuscript.

Funding: This research was funded by the German Federal Ministry for Economic Affairs and Climate Action (BMWK), grant number 03EI3046A.

Data Availability Statement: The authors confirm that the data supporting the findings of this study are available within the article.

Conflicts of Interest: The authors declare no conflict of interest.

References

1. Kasavajjula, U.; Wang, C.; Appleby, A.J. Nano-and bulk-silicon-based insertion anodes for lithium-ion secondary cells. *J. Power Sources* **2007**, *163*, 1003. [[CrossRef](#)]
2. Su, X.; Wu, Q.; Li, J.; Xiao, X.; Lott, A.; Lu, W.; Sheldon, B.W.; Wu, J. Silicon-Based Nanomaterials for Lithium-Ion Batteries: A Review. *Adv. Energy Mater.* **2014**, *4*, 1300882. [[CrossRef](#)]
3. Obrovac, M.N.; Chevrier, V.L. Alloy Negative Electrodes for Li-Ion Batteries. *Chem. Rev.* **2014**, *114*, 11444. [[CrossRef](#)] [[PubMed](#)]
4. Jin, Y.; Zhu, B.; Lu, Z.; Liu, N.; Zhu, J. Challenges and Recent Progress in the Development of Si Anodes for Lithium-Ion Battery. *Adv. Energy Mater.* **2017**, *7*, 1700715. [[CrossRef](#)]
5. Graf, M.; Berg, C.; Bernhard, R.; Haufe, S.; Pfeiffer, J.; Gasteiger, H.A. Effect and Progress of the Amorphization Process for Microscale Silicon Particles under Partial Lithiation as Active Material in Lithium-Ion Batteries. *J. Electrochem. Soc.* **2022**, *169*, 020536. [[CrossRef](#)]
6. Gonzalez, J.; Sun, K.; Huang, M.; Lambros, J.; Dillon, S.; Chasiotis, I. Three dimensional studies of particle failure in silicon based composite electrodes for lithium ion batteries. *J. Power Sources* **2014**, *269*, 334. [[CrossRef](#)]
7. Liu, X.H.; Zhong, L.; Huang, S.; Mao, S.X.; Zhu, T.; Huang, J.Y. Size-Dependent Fracture of Silicon Nanoparticles during Lithiation. *ACS Nano* **2012**, *6*, 1522. [[CrossRef](#)] [[PubMed](#)]
8. Luo, F.; Liu, B.; Zheng, J.; Chu, G.; Zhong, K.; Li, H.; Huang, X.; Chen, L. Nano-silicon/carbon composite anode materials towards practical application for next generation Li-ion batteries. *J. Electrochem. Soc.* **2015**, *162*, A2509. [[CrossRef](#)]
9. Marom, S.F.A.R.; Leifer, N.; Jacob, D.; Aurbach, D. A review of advanced and practical lithium battery materials. *J. Mater. Chem.* **2011**, *21*, 9938. [[CrossRef](#)]
10. Peled, E.; Menkin, S. SEI: Past, present and future. *J. Electrochem. Soc.* **2017**, *164*, A1703. [[CrossRef](#)]
11. Goriparti, S.; Miele, E.; De Angelis, F.; Di Fabrizio, E.; Zaccaria, R.P.; Capiglia, C. Review on recent progress of nanostructured anode materials for Li-ion batteries. *J. Power Sources* **2014**, *257*, 421. [[CrossRef](#)]
12. Takezawa, H.; Iwamoto, K.; Ito, S.; Yoshizawa, H. Electrochemical behaviors of nonstoichiometric silicon suboxides (SiO_x) film prepared by reactive evaporation for lithium rechargeable batteries. *J. Power Sources* **2013**, *244*, 149. [[CrossRef](#)]
13. Chevrier, V.L.; Liu, L.; Le, D.B.; Lund, J.; Molla, B.; Reimer, K.; Krause, L.J.; Jensen, L.D.; Figgemeier, E.; Eberman, K.W. Evaluating Si-based materials for Li-ion batteries in commercially relevant negative electrodes. *J. Electrochem. Soc.* **2014**, *161*, A783. [[CrossRef](#)]
14. Heist, A.; Piper, D.M.; Evans, T.; Kim, S.C.; Han, S.S.; Oh, K.H.; Lee, S.-H. Self-Contained Fragmentation and Interfacial Stability in Crude Micron-Silicon Anodes. *J. Electrochem. Soc.* **2018**, *165*, A244. [[CrossRef](#)]
15. Kim, H.; Han, B.; Choo, J.; Cho, J. Three-dimensional porous silicon particles for use in high-performance lithium secondary batteries. *Angew. Chem. Int. Ed.* **2008**, *120*, 10305. [[CrossRef](#)]
16. Wang, C.; Chui, Y.-S.; Ma, R.; Wong, T.; Ren, J.-G.; Wu, Q.-H.; Chen, X.; Zhang, W. A three-dimensional graphene scaffold supported thin film silicon anode for lithium-ion batteries. *J. Mater. Chem. A* **2013**, *1*, 10092. [[CrossRef](#)]
17. Zuo, X.; Zhu, J.; Müller-Buschbaum, P.; Cheng, Y.-J. Silicon based lithium-ion battery anodes: A chronicle perspective review. *Nano Energy* **2017**, *31*, 113. [[CrossRef](#)]
18. Müller, V.; Bernhard, R.; Wegener, J.; Pfeiffer, J.; Rössler, S.; Scurtu, R.; Memm, M.; Danzer, M.A.; Wohlfahrt-Mehrens, M. Evaluation of Scalable Porous Si-Rich Si/C Composites with Low Volume Expansion in Coin Cells to Prismatic Cell Formats. *Energy Technol.* **2020**, *8*, 2000217. [[CrossRef](#)]
19. Obrovac, M.N.; Krause, L.J. Reversible Cycling of Crystalline Silicon Powder. *J. Electrochem. Soc.* **2007**, *154*, A103. [[CrossRef](#)]
20. Nguyen, B.P.N.; Chazelle, S.; Cerbelaud, M.; Porcher, W.; Lestriez, B. Manufacturing of industry-relevant silicon negative composite electrodes for lithium ion-cells. *J. Power Sources* **2014**, *262*, 112. [[CrossRef](#)]
21. Beattie, S.D.; Loveridge, M.J.; Lain, M.J.; Ferrari, S.; Polzin, B.J.; Bhagat, R.; Dashwood, R. Understanding capacity fade in silicon based electrodes for lithium-ion batteries using three electrode cells and upper cut-off voltage studies. *J. Power Sources* **2016**, *302*, 426. [[CrossRef](#)]
22. Jantke, D.; Bernhard, R.; Hanelt, E.; Buhrmester, T.; Pfeiffer, J.; Haufe, S. Silicon-Dominant Anodes Based on Microscale Silicon Particles under Partial Lithiation with High Capacity and Cycle Stability. *J. Electrochem. Soc.* **2019**, *166*, A3881. [[CrossRef](#)]
23. Haufe, S. Siliciumpartikel enthaltende Anodenmaterialien für Lithium-Ionen-Batterien. Patent. EP 3335262 B1, 28 July 2016.

24. Wagner, N.P.; Tron, A.; Tolchard, J.R.; Noia, G.; Bellmann, M.P. Silicon anodes for lithium-ion batteries produced from recovered kerf powders. *J. Power Sources* **2019**, *414*, 486. [[CrossRef](#)]
25. Haufe, S.; Bernhard, R.; Pfeiffer, R. Revealing the Failure Mechanism of Partially Lithiated Silicon-Dominant Anodes Based on Microscale Silicon Particles. *J. Electrochem. Soc.* **2021**, *168*, 080531. [[CrossRef](#)]
26. Zhang, S.; Andreas, N.S.; Li, R.; Zhang, N.; Sun, C.; Lu, D.; Gao, T.; Chen, L.; Fan, X. Mitigating irreversible capacity loss for higher-energy lithium batteries. *Energy Storage Mater.* **2022**, *48*, 44. [[CrossRef](#)]
27. Buchberger, I.; Jantke, D.; Haufe, S. Lithium Ion. Batteries. Patent WO 2020211938 A1, 17 April 2019.
28. Nguyen, C.C.; Yoon, T.; Seo, D.M.; Guduru, P.; Lucht, B.L. Systematic Investigation of Binders for Silicon Anodes: Interactions of Binder with Silicon Particles and Electrolytes and Effects of Binders on Solid Electrolyte Interphase Formation. *ACS Appl. Mater. Interfaces* **2016**, *8*, 12211. [[CrossRef](#)]
29. Jung, R.; Metzger, M.; Haering, D.; Solchenbach, S.; Marino, C.; Tsiouvaras, N.; Stinner, C.; Gasteiger, H.A. Consumption of fluoroethylene carbonate (FEC) on Si-C composite electrodes for Li-ion batteries. *J. Electrochem. Soc.* **2016**, *163*, A1705. [[CrossRef](#)]
30. Bernhard, R.; Haufe, S.; Ege, M. Lithium Ion. Batteries. Patent WO 2020233799 A1, 21 May 2019.
31. Holtstiege, F.; Bärman, P.; Nölle, R.; Winter, M.; Placke, T. Pre-lithiation strategies for rechargeable energy storage technologies: Concepts, promises and challenges. *Batteries* **2018**, *4*, 4. [[CrossRef](#)]
32. Xin, C.; Gao, J.; Luo, R.; Zhou, W. Prelithiation Reagents and Strategies on High Energy Lithium-Ion Batteries. *Chem. Eur. J.* **2022**, *28*, e202104282. [[CrossRef](#)]
33. Huang, Z.; Deng, Z.; Zhong, Y.; Xu, M.; Li, S.; Liu, X.; Huang, K.; Shen, Y.; Huang, Y. Progress and challenges of prelithiation technology for lithium-ion battery. *Carbon Energy* **2022**, *4*, 1107. [[CrossRef](#)]
34. Dose, W.M.; Johnson, C.S. Cathode pre-lithiation/sodiation for next-generation batteries. *Curr. Opin. Electrochem.* **2022**, *31*, 100827. [[CrossRef](#)]
35. Chevrier, V.L.; Liu, L.; Wohl, R.; Chandrasoma, A.; Vega, J.A.; Eberman, K.W.; Figgemeier, E. Design and Testing of Prelithiated Full Cells with High Silicon Content. *J. Electrochem. Soc.* **2018**, *165*, A1129. [[CrossRef](#)]
36. Dimov, N.; Kugino, S.; Yoshio, M. Carbon-coated silicon as anode material for lithium ion batteries: Advantages and limitations. *Electrochim. Acta* **2003**, *48*, 1579. [[CrossRef](#)]
37. Wegener, J.; Haufe, S.; Stohrer, J. Carbon-Coated Silicon Particles for Lithium Ion Batteries. EP 3535793 B1, 11 January 2017.
38. Li, Y.; Yan, K.; Lee, H.-W.; Lu, Z.; Liu, N.; Cui, Y. Growth of conformal graphene cages on micrometre-sized silicon particles as stable battery anodes. *Nat. Energy* **2016**, *1*, 15029. [[CrossRef](#)]
39. Lu, Z.; Liu, N.; Lee, H.-W.; Zhao, J.; Li, W.; Li, Y.; Cui, Y. Nonfilling Carbon Coating of Porous Silicon Micrometer-Sized Particles for High-Performance Lithium Battery Anodes. *ACS Nano* **2015**, *9*, 2540. [[CrossRef](#)] [[PubMed](#)]
40. Graf, M.; Reuter, L.; Qian, S.; Calmus, T.; Ghamlouche, A.; Maibach, J.; Bernhard, R.; Gasteiger, H.A. Understanding the Effect of Lithium Nitrate as Additive in Carbonate Based Electrolytes for Silicon Anodes. In *ECS Meeting Abstracts*; IOP Publishing: Bristol, UK, 2021. [[CrossRef](#)]
41. Stearns, L.A.; Gryko, J.; Diefenbacher, J.; Ramachandran, G.K.; McMillan, P.F. Lithium monosilicide (LiSi), a low-dimensional silicon-based material prepared by high pressure synthesis: NMR and vibrational spectroscopy and electrical properties characterization. *J. Solid State Chem.* **2003**, *173*, 251. [[CrossRef](#)]

Disclaimer/Publisher's Note: The statements, opinions and data contained in all publications are solely those of the individual author(s) and contributor(s) and not of MDPI and/or the editor(s). MDPI and/or the editor(s) disclaim responsibility for any injury to people or property resulting from any ideas, methods, instructions or products referred to in the content.